

**Arsenic release and attenuation in a multilayer aquifer in the Po Plain (northern Italy):
reactive transport modeling**

*Marco Rotiroti^{*a}, Rasmus Jakobsen^b, Letizia Fumagalli^a and Tullia Bonomi^a*

^aDepartment of Earth and Environmental Sciences, University of Milano-Bicocca, Piazza della Scienza 1, 20126 Milan, Italy.

^bGEUS-Geological Survey of Denmark and Greenland, Øster Voldgade 10, 1350 Copenhagen, Denmark.

*corresponding author, email: m.rotiroti@campus.unimib.it, tel: +39 0264482882, fax: +39 0264482895.

Applied Geochemistry (2015), doi:10.1016/j.apgeochem.2015.07.001

Received Date: 13 March 2015; Revised Date: 29 June 2015; Accepted Date: 8 July 2015

For the full version go to

<http://www.sciencedirect.com/science/article/pii/S0883292715300068?np=y#>

Abstract

Groundwater As concentrations > WHO limit (10 µg/L) are frequently found in the Po Plain (N. Italy). Although several hypotheses on As mobilization exist (i.e., reductive dissolution driven by peat degradation), the mechanisms of As release and subsequent attenuation acting in the multilayer aquifer in the Po Plain were poorly understood.

The present work aims at implementing a reactive transport modeling of the aquifer system in Cremona, affected by As < 183 µg/L, in order to quantify and test the feasibility of As release by the reductive dissolution of Fe-oxides driven by the degradation of peat contained in leaky aquitards and As attenuation downstream by the co-precipitation in iron sulfides.

The model, based on a partial equilibrium approach, revealed that the observed As, Fe and Mn chemistry could be mostly explained by the simultaneous equilibrium between Fe-oxide and sulfate reduction and FeS precipitation and by the equilibrium of rhodochrosite precipitation/dissolution. Model results, together with litholog analysis, supported the assumption of peat as the likely source of organic matter driving As release. The model fitted to measured data showed that the peak in the organic carbon degradation rate at 20-40 m below surface (average of 0.67 mM/y), corresponding to the shallow peaty aquitard and the upper portion of the underlying semiconfined aquifer, is associated with the peak of net release of As (average of 0.32 $\mu\text{M}/\text{y}$) that is followed just downstream by a net precipitation in iron sulfides at 40-60 m below surface (average of 0.30 $\mu\text{M}/\text{y}$). These results support the assumptions of peaty aquifers as drivers of As release and iron sulfides as As traps. The model also outlined the following aspects that could have a broad applicability in other alluvial As affected aquifers worldwide: (a) shallow peaty aquitards may have a greater role in driving the As release since they likely have young and more reactive organic matter; (b) the occurrence of Fe-oxide reduction and FeS precipitation, that represent the As source and sink, together with sulfate reduction occurring simultaneously close to equilibrium may restrict the As mobility limiting the extent of contamination just downstream the source of organic matter that drives its release.

Keywords: Reactive Transport Modeling; Peat; Aquitard; Iron Sulfide; As Mobility; Cremona.

1. Introduction

Arsenic affected groundwater is known to be a serious problem for human health due to its direct utilization for drinking supply in many regions worldwide (Ravenscroft et al. 2009). However, in the last few years, the attention was also focused on human exposure to As through food (Sharma et al. 2014) since As rich groundwater is used for crop irrigation (de la Fuente et al. 2010; Huq et al.

2006) and preparation of food items, e.g., cooking (Díaz et al. 2004; Torres-Escribano et al. 2008). In the Po Plain (northern Italy, 46 000 km² and ~20 million inhabitants), the health risk of As related to drinking water is currently low since groundwater is treated, lowering As concentration to <10 µg/L. However, until 2000, groundwater had no purification, leading to average As concentrations in drinking water up to 70 µg/L, with maxima up to 190 µg/L (data for Lombardy Region; Castelli et al. 2005). A higher risk may be related to As entering the food chain since previous studies reported higher average As concentrations in rice and wheat cultivated in the Po Plain with respect to other Italian regions with no As affected groundwater, i.e., 230 against 110 µg/kg for Calabria Region, southern Italy, in rice (Sommella et al. 2013) and 10.1 against 8.2 and 8.3 µg/kg for central and southern Italy, respectively, in wheat (Cubadda et al. 2010). Moreover, another indication of the diffuse environmental contamination by As in the Po Plain can be given by its average concentration in Po River waters of 12 µg/L (Marchina et al. 2015), that exceeds the WHO limit of 10 µg/L, most likely related to the inflow of As bearing groundwater into the river (Rotiroti et al. 2014). On this background, the identification of the mechanisms of As release into groundwater in the Po Plain becomes a key for directing water policies to reduce the health risk of this geogenic contaminant.

Previous studies pointed out that high As concentrations in groundwater in the Po Plain are found in semiconfined and confined aquifers under reduced conditions, generally between 50 and 120 m below surface (b.s.) (Molinari et al. 2013; Rotiroti et al. 2014; Zavatti et al. 1995). In particular, Rotiroti et al. (2014) suggested the reductive dissolution of iron oxides (Ravenscroft et al. 2009) driven by peat degradation as the primary mechanism of As release. Peat is commonly found in the lower part of the Po Plain, mostly related to fine-grained deposits acting as semipermeable aquitards (Amorosi et al. 2005; Amorosi et al. 2008; Baraldi et al. 2001; Miola et al. 2006). Peats were likely formed in abandoned meanders and zones of water stagnation generated by major river courses (Baraldi et al. 2001) and buried by subsequent alluvial depositions and incorporated into the stratigraphic sequence (Miola et al. 2006). Although peaty aquitards seem to be responsible for As

release in the Po Plain, together with other reduced species such as Fe, Mn, NH₄ and CH₄ (Carraro et al. 2013; Rotiroti et al. 2014; Sciarra et al. 2013; Zavatti et al. 1995), no thorough analyses were addressed at substantiating this hypothesis. Recent studies regarding other alluvial basins worldwide, particularly the Bengal Basin, highlighted the key role played by peaty aquitards on As release to surrounding aquifers (Desbarats et al. 2014; Planer-Friedrich et al. 2012). In particular, Desbarats et al. (2014) implemented a simplified 1D vertical reactive transport model to simulate the flushing of As from source sediments (i.e., a peaty aquitard) to the underlying aquifer considering a simple phenomenological representation of As release. The present work aims to test the As release from a peaty aquitard to the underlying aquifer in the Po Plain considering the reductive dissolution of Fe-oxides as mobilization mechanism by implementing a 1D vertical reactive transport model.

Moreover, it was found that in the Po Plain the evolution over depth of As concentrations is characterized by a decrease below 120-150 m b.s. (Carraro et al. 2013; Guffanti et al. 2010; Rotiroti et al. 2014). This could be due the co-precipitation of As in newly formed iron sulfides (Rotiroti et al. 2014; Zavatti et al. 1995). In addition, Toscani et al. (2007) suggested that Fe concentrations in Fe-rich groundwater in the Po Plain are controlled by iron sulfides and siderite precipitation. The sequestration of As by co-precipitation in iron sulfides was identified as a mechanism of As attenuation in other alluvial systems (Buschmann and Berg 2009; Fendorf et al. 2010; Lowers et al. 2007; Root et al. 2009).

In summary, the reactive transport modeling presented in this work aims to check the feasibility in the Po Plain of (a) the As release from a peaty aquitard to the underlying aquifer by the reductive dissolution of Fe-oxides and (b) the precipitation of iron sulfides as a trap for groundwater As. To the best of our knowledge, no other studies implemented a reactive transport modeling of both As release from the reductive dissolution of Fe-oxides and As sequestration by the co-precipitation in iron sulfides along the same flowpath.

The present work involved (a) the aquifer characterization by a reconstruction of the 3D distribution of hydraulic conductivity (K), effective porosity and textural facies, (b) the identification of likely processes governing the hydrogeochemistry of the system and (c) the implementation of a 1D reactive transport modeling to check feasibility and quantify the hydrogeochemical conceptual model proposed (Rotiroti et al. 2014).

2. Materials and methods

2.1. Study Area

The study area covers 150 km² in and around the town of Cremona (N. Italy) close to the Po River (Figure 1a). This area is the same investigated in the previous work by Rotiroti et al. (2014). The subsurface is formed by Holocene and Pleistocene alluvial deposits and hosts a multilayer aquifer composed of five aquifer subunits: aquifers U (0-25 m b.s.), S (30-50 m b.s.), C1 (65-85 m b.s.), C2 (100-150 m b.s.) and C3 (160-260 m b.s.). Groundwater has a component of downward flow from aquifer U to C2 and upward flow from C3 to C2 (Rotiroti et al. 2014). Aquifer U has a redox zoning (a zone with more oxidized conditions, called U_{ox}, a zone with more reduced conditions, called U_{red}, and a zone with intermediate conditions, called U_{mix}), whereas the underlying aquifers (S, C1, C2 and C3) are all anoxic (Rotiroti and Fumagalli 2013; Rotiroti et al. 2014).

2.2. Aquifer Characterization

The 3D distribution of textural facies, hydraulic conductivity and effective porosity was reconstructed using geostatistics. The 553 lithologs from boreholes located in and around the study area, that are stored in the TANGRAM database (Bonomi et al. 2014), were coded (Bonomi 2009) and interpolated by kriging through a quasi-3D stratified approach (Fabbri and Trevisani 2005)

using GOCAD (Paradigm 2009). Details are reported in the Supporting Information. In addition, a representation of peat deposits in the aquifer system was realised by a 3D map reporting its content (percentage of peat over all other reported lithologies) in the collected lithologies (Figure 2). It should be noted that this representation underestimates the real distribution of peat due to the following considerations: (a) in areas without boreholes the presence of peat cannot be inferred; (b) lithologies were made by different well loggers in different years and with different degrees of accuracy, therefore, in some cases, peat could have been detected but not recorded by inexperienced loggers.

2.3. Speciation and Mineral Saturation

The present work is based on 66 groundwater samples collected in July 2010 for major ions and trace elements analyses (Rotiroti et al. 2014). Conventional sampling and analytical methods were applied (see Rotiroti et al. 2014 for details). The samples were measured in triplicate, yielding average precisions of 2% for NH_4 , 5% for major ions, Fe and Mn and 10% for As and accuracies of 5% for NH_4 and 10% for major ions and trace elements.

Hydrochemical data were treated using PHREEQC (Parkhurst and Appelo 2013) with the wateq4f database (Ball and Nordstrom 1991) to calculate speciation and mineral saturation indexes (SIs). Speciation was computed using pe values calculated from field ORP measurements (Rotiroti et al. 2014). The average pe value for each aquifer was used for samples with missing measurement.

2.4. Redox Processes

The identification of the main redox processes governing the system was based on the partial equilibrium approach proposed by Postma and Jakobsen (1996) that splits the degradation of organic matter (OM) into two steps: (a) the hydrolyzation and fermentation of OM with the production of simpler compounds, e.g., formic acid, acetic acid, H_2 and CO_2 and (b) the

consumption of the fermentative products by different terminal electron accepting processes (TEAPs). The first step controls the overall rate whereas TEAPs are assumed to approach equilibrium. This approach is applicable for Mn-oxide, Fe-oxide and sulfate reduction and methanogenesis, whereas it is not adequate for oxygen and nitrate reduction which involves a likely direct metabolization of the OM by microorganisms (Appelo and Postma 2005).

The occurrence of TEAPs near equilibrium was tested by plotting the measured data on chemical equilibrium diagrams (i.e., logarithmic activity plots with equilibrium lines). The following equilibrium system were considered: (a) simultaneous equilibrium of Fe-oxide and sulfate reduction and FeS precipitation (Postma and Jakobsen 1996), (b) simultaneous equilibrium of Fe-oxide and sulfate reduction and FeS and siderite precipitation and (c) equilibrium of Mn-oxides reduction. In order to check the role played by other reactions that could control the Fe^{2+}/pH and Mn^{2+}/pH relations, equilibrium control by siderite and rhodochrosite was also examined. Details on the stoichiometry of these reactions are reported in the Supporting Information.

2.5. Transport Model Settings

We implemented a 1D reactive transport model using PHREEQC considering a downward flow through a vertical column composed by 12 cells of 10 m that represents the first 120 m of depth comprising the first three aquifers (i.e., U, S and C1). The length of the cell was chosen on the basis of the average screen length of the wells used for the model calibration (see Sect. 2.6), that is 10.3 m, since the SIs of minerals near equilibrium, calculated from the measured groundwater compositions of these wells, were imposed as geochemical boundary conditions in the model (Jakobsen and Cold 2007). A more refined grid (e.g., 1 m cell length) did not increase the quality of model results (see the Supporting Information for details).

The choice of a 1D modeling is justified by the following consideration. First, the main aim of this modeling is to support the hydrogeochemical conceptual model of As release and attenuation rather

than to reconstruct complex 3D concentration distributions, therefore we tried to keep the model as simple as possible in order to minimize the quantity of input values needed and the computational requirements. Second, we decided to calibrate the model using the measured concentrations in the eastern part of the study area (see Sect. 2.6) because here, unlike in other parts, the K distribution (see Sect. 3.1) shows the presence of discontinuous and more conductive aquitards (silty sands) allowing the system to be approximated by a coherent groundwater body (at least for aquifers U, S and C1). Third, the previous study by Rotiroti et al. (2014) showed that no significant variation of redox features is seen within the same aquifer unit (i.e., same range of depth) with the exception of aquifer U where three zones were identified (i.e., Ured, Uox and Umix), so the projection of data on a vertical 1D transect can be sustained (the data from aquifer U in the eastern part of the study area, that were used for the model calibration, are all from Ured). Moreover, only including the first three aquifers is justified by the hydrodynamics of the system: groundwater flows downwards from aquifer U to C2 but upwards from C3 to C2. Aquifer C2 was excluded from the modeling due to a possible mass flow coming from the bottom (i.e., from aquifer C3). A scheme of the geometry of the model is shown in Table 1. Depths and thickness of aquifer and aquitard layers are average values derived from Section 1-1' in Figure 1b considering mostly the hydrogeological settings close to the sampled wells.

The transport was simulated for steady-state flow with a constant vertical flow from the top to the bottom of the column. The vertical flow velocity of 3.12 m/y was calculated from measured hydraulic heads and modeled hydraulic conductivity and effective porosity values (see the Supporting Information). No dispersion was considered because it seems to play a minor role in the vertical flow (Postma et al. 2007), whereas a diffusion coefficient of $0.3 \times 10^{-9} \text{ m}^2/\text{s}$ (i.e., the PHREEQC default value) was included. A total period of 160 years ($\sim 4 \times$ the travel time of the solution through the column) was modeled. After ~ 40 years, when 1 pore volume has flushed the system, the biogeochemistry of the system reached a quasi-steady-state. The model was left to run for other 120 years allowing the system to be further flushed by 3 pore volumes in order to ensure

the approach to a likely steady As distribution (see below). In order to effectively check the negligible role of vertical dispersion in this modeling, a sensitivity analysis was performed considering 5 different dispersivity values (0.0001, 0.001, 0.01, 0.1, 1 m) that cover the reported range by Gelhar et al (1992). Results (see the Supporting Information) showed that, in general, the use of any vertical dispersivity values did not significantly change the model results.

The chemistry included in the model system is based on the hydrogeochemical conceptual model proposed by Rotiroti et al. (2014) and results of mineral saturation and redox processes analyses. The system includes I) equilibrium reactions: (a) the reductive dissolution of Fe-oxide with trace As(V), (b) the precipitation of calcite, dolomite, siderite and rhodochrosite and (c) the precipitation of FeS with trace As(III) and II) irreversible reactions: (a) oxidation of OM (i.e., peat) as $(\text{CH}_2\text{O})_{106}(\text{NH}_3)_{4.5}(\text{H}_3\text{PO}_4)$, producing inorganic C, NH_4^+ and inorganic P and (b) the reductive dissolution of Mn-oxide. The composition of OM used in the model was obtained starting from the Redfield ratio (Redfield 1934) and then adjusting the molar content of NH_3 by fitting modeled to measured NH_4 concentrations. In particular for As, the model considered only an Fe-oxide with trace amount of arsenic as its source in groundwater. Mn-oxides were not defined as a source of As due to the most likely resorption to Fe-oxides (McArthur et al. 2004). Concerning the sink for dissolved As, the model considered the co-precipitation in iron sulfides (Buschmann and Berg 2009; Lowers et al. 2007; Root et al. 2009). On the basis of the reductive dissolution mechanism (Ravenscroft et al. 2009), the arsenic released from the Fe-oxide was set as As(V), which is reduced and coprecipitated in FeS as As(III). We decided to neglect any surface complexation models (SCMs) for the following reasons: (a) the hydrogeochemical conceptual model considered the reductive dissolution of Fe-oxides and the co-precipitation in FeS as the main processes responsible for the net release and attenuation of As; these processes cannot be properly modeled by a SCM since the former implies the destruction of the sorption sites for As and the latter involves the inclusion of As into the FeS structure and not the As adsorption on the FeS surface; (b) considering that the processes simulated by a SCM (i.e., As adsorption/desorption on/from Fe-oxides and,

maybe, on/from Mn-oxides) seem to play a minor role in the net As release and attenuation in the Cremona area, the proposed modeling was kept as simple as possible in order to minimize the model uncertainty; therefore a SCM was omitted in order to avoid the increasing of model uncertainty for processes considered of minor importance in the system (the uncertainty is related to the choice of the model (Jessen et al. 2012) and their input data, as sorption sites density, etc.); (c) the work of Postma et al. (2007), that considered a SCM for the sorption of As on the Fe-oxides, pointed out that when the supply of As from the reductive dissolution reached a quasi-steady-state (in that case, after 2 pore volumes flushed) the sorption of As on the Fe-oxides had no further retarding effect on the As transport. The Cremona system is much older than the system modeled by Postma et al. (2007), at least below aquifer U, making it reasonable to assume that the system is close to a steady-state also with regards to sorption.

The composition of the initial solutions (i.e., the solution in the cells at time zero) and solution zero (i.e., solution that enters the column at every time step) were based on a shallow sample from aquifer U (see the Supporting Information for details). The imposed SI values, considered as geochemical boundary conditions, varied within each aquifer and aquitard unit and they were adjusted as part of the model calibration (see the Supporting Information for details).

2.6. Transport Model Calibration

The model was calibrated by fitting modeled concentrations to the field data as done in previous 1D and 2D reactive transport modeling (Jakobsen and Cold 2007; Jakobsen and Postma 1999; Postma et al. 2007; Sigfusson et al. 2011). A subset of the measured data, composed of samples from wells located in the eastern part of the study area that tap aquifer U to C1 (a total of 8 wells; see the Supporting Information for details), was used for the calibration. In this zone, the system comprised of aquifers U and C1 can be considered as a coherent groundwater body making the 1D approximation acceptable (see Sect. 2.5). The As concentrations measured in the eastern part of the

area are shown in Figure 1b as a projection of the wells sampled onto a N/S cross-section of K values (cross-section 1-1'); the wells are further projected into a 1D column.

The model was sensitive to the following parameters: (a) the rate of OM degradation, (b) the SI of the Fe-oxide, that controls its stability, and (c) the SI of the FeS. The rate of OM degradation was calibrated considering the fitting between simulated and measured ammonium data (the ammonium being released from the reacting OM), which could be considered conservative due to the anoxic conditions of the system. The C/N ratio of OM was set to 23.6. This value is the optimal result of an iterative approach testing different C/N ratios starting from the value of 15.1 (Postma et al. 2007) and using the matching between NH_4 measured and released in the model as guidance. The SI of the Fe-oxide was used to control the concentration of Fe^{3+} , that is further reduced in the reaction with the OM, and therefore to calibrate the Fe^{2+} concentration indirectly. The SI of the FeS, which has trace As, was used to control its precipitation, and thus, to calibrate the dissolved As concentration. Moreover, the As concentration was also controlled by the content of As in the Fe-oxide and FeS. A constant As(V)/Fe molar ratio in the Fe-oxide of 4.5×10^{-4} and a variable As(III)/Fe molar ratio in the FeS with a maximum of 2.0×10^{-2} were considered. These values gave the best model fit to measured data. The As(V)/Fe ratio of 4.5×10^{-4} is consistent with the value of 8.0×10^{-4} measured by oxalate extractions and 2.5×10^{-3} used in the reactive transport model in the Red River floodplain (Postma et al. 2007). The maximum As(III)/Fe ratio of 2.0×10^{-2} approaches that measured by Lowers et al. (2007) in pyrite samples from the Bengal Basin (i.e., maximum of 1.9×10^{-2}). The variable As(III)/Fe ratio in the FeS was obtained considering two different FeS phases: the former is pure FeS and the latter is FeS with trace As in a constant As(III)/Fe ratio of 2.0×10^{-2} . These two different FeS phases were defined to allow the FeS precipitation also when As concentration was low (i.e., when As concentration was not sufficient to reach the As(III)/Fe ratio of 2.0×10^{-2}). Since a quasi-steady-state and no kinetics were considered, the modeled concentrations were not sensitive to the flow velocity. This parameter only affected the absolute value of modeled rates while leaving the shape of the depth profile.

3. Results

3.1. Hydraulic Conductivity and Peat Distribution

Figure 1a shows the 3D distribution of the hydraulic conductivity in the study area (see the Supporting Information for results of textural facies and effective porosity). The eastern part of the study area (Figure 1a, cross-section 1-1') has consistent sandy layers (K of 60-130 m/d) that are mainly separated by semipermeable aquitards (K of 0.5-5 m/d) and more rarely by clayey low-permeability layers (K of 9.6×10^{-3} - 3.8×10^{-2} m/d). The central part (Figure 1a, cross-section 2-2') shows sandy layers with generally lower thickness and conductivity (K of 40-90 m/d) that tend to be sharply separated by clayey layers (K of 8.6×10^{-3} - 3.8×10^{-2} m/d) and, more rarely, by semipermeable aquitards (K of 0.5-5 m/d). The western part (Figure 1a, cross-section 3-3') reveals intermediate conditions with a dominant content of silty sands (K of 0.5-5 m/d). Sandy layers have generally lower conductivity (K of 30-80 m/d) and are occasionally separated by clayey layers (K of 8.6×10^{-3} - 3.8×10^{-2} m/d). It is noted that, unlike in the other parts, the aquifers in the eastern zone are found to be less separated (i.e., smaller extent of clayey layers and frequent occurrence of silty sands) even being in direct contact at certain locations (e.g., aquifers U and S at well 69 and aquifers S and C1 at wells 51 and 70). Figure 2 shows that peat is commonly found in the study area. It is almost always associated with clayey and silty deposits.

3.2. Mineral Dissolution and Redox Processes

The SIs indicated that groundwater is slightly supersaturated with respect to calcite and dolomite (average SI of 0.65 and 0.71, respectively) and near equilibrium with rhodochrosite and siderite

(average SI of -0.13 and -0.12, respectively). This is clearly shown in Figure 3 by the equilibrium diagrams for dissolution/precipitation of the four carbonates considered.

Figure 4a shows the diagram of the simultaneous equilibrium of Fe-oxide and sulfate reduction and FeS precipitation (black solid lines). Most of the data are aligned along a slope similar to the equilibrium lines. The equilibrium line of a hypothetical Fe-oxide that fits the data is plotted in the diagram (black dotted line). This line considers a solubility product of Fe-oxide for which $\log K = 0.78$ (41.19 considering the alternative representation of the solubility product; Cornell and Schwertmann 2003) that is in the range of stability of goethite (Appelo and Postma 2005) and may represent a microcrystalline goethite. The red lines in Figure 4a show the equilibrium lines for simultaneous equilibrium of Fe-oxide and sulfate reduction and FeS and siderite precipitation. The two types of equilibrium lines (with or without siderite) differ only slightly. This implies that it is difficult to distinguish a system controlled by just equilibrium with FeS from a system controlled by both FeS and siderite.

The equilibrium diagram for Mn-oxides reduction is shown in Figure 4b. The equilibrium lines for birnessite and pyrolusite reduction (black solid lines) are far from the measured data. The equilibrium lines are still far from the data considering also a higher pe value, for example equal to 5 (closer to the maximum measured value, i.e., 4.81; black dotted line in Figure 4b). Moreover, the slope of the equilibrium lines clearly differs from that of the data alignment.

3.3. 1D Reactive Transport Modeling

Figure 5 shows (a) the measured and modeled concentrations of some major ions and redox sensitive species over depth and (b) the modeled rates of organic carbon (OC) degradation and main processes involving iron, manganese and arsenic (see Table 1 and the Supporting Information for details).

Modeled ammonium concentrations could only be fitted to measured data by imposing a higher rate of OC degradation from cell 3 to 5 (i.e., 20-50 m b.s.) corresponding to the aquitard between aquifers U and S (aquitard U/S) and the upper part of aquifer S (Table 1). The average OC degradation rate in these three cells is 0.55 mM/y, a value that is consistent with previous studies (Appelo and Postma 2005). The average OC oxidation rate for the whole model (12 cells) is 0.14 mM/y, in line with the constant value of 0.15 mM/y used by Postma et al. (2007) in their modeling. Modeled Fe^{2+} and SO_4 concentrations matched their observed vertical profiles (i.e., an increase up to 20-30 m b.s. and a downward decrease for Fe^{2+} and an exponential decrease down to 50 m b.s. for SO_4) considering a stability of Fe-oxide of $\log K = -0.11$. Modeled rates show that the peaks of Fe-oxide and SO_4 reduction correspond to the highest OC degradation rate in cell 4. Siderite precipitation has a first peak in cell 3, then a slight decrease in cell 4 where the peak in sulfate reduction favors the formation of FeS, and a second peak in cell 5 where sulfate reduction decreases. The modeled pH has a general increase over depth, consistent with the measured values, with a local decrease in cell 4 where the rates of OC degradation, Fe-oxide and sulfate reduction are the highest. The net Fe^{2+} rates show that its highest release is in cell 3, where OC degradation and Fe-oxide reduction have the first increase. In the underlying cells the net release of Fe^{2+} decreases down to cell 5. From cell 6 to 8, the rate reflects a net precipitation of Fe^{2+} in siderite (mostly) and FeS.

The model approached the observed Mn^{2+} profile (i.e., a peak between 20 and 50 m b.s. and a downward decrease) implying the highest rate of Mn-oxide reductive dissolution, via OC, in cell 4, where the rate of OC degradation has the peak. The modeled rate of rhodochrosite precipitation has a peak in cell 3, where Mn-oxide reduction starts to increase, then decreases over depth. The net Mn^{2+} rates indicate a prevailing precipitation starting from cell 3 that continues downward with decreasing values.

Modeled As concentrations matched the observed values (i.e., an increase up to 30-40 m b.s. and a downward decrease) imposing the As(III)/Fe molar ratio in total FeS (as the sum of the two phases)

with an increasing value from cell 3 to 6 (from 2.0×10^{-4} to 2.0×10^{-2}) and a constant value of 2.0×10^{-2} in the underlying cells (Table 1). The rate of As(V) release is higher in cell 4, coinciding with the peak of Fe-oxide reduction, whereas the precipitation of As(III) has the highest rate in cell 5, where the As(III)/Fe ratio in FeS has a strong increase (from 0 in cell 4 to 1.9×10^{-2} in cell 5). The net As rates (Table 1) show that As is mainly released in cells 3 and 4 due to the reductive dissolution of Fe-oxide and mainly removed in cells 5 and 6 due to the co-precipitation in FeS. Release of As is prevalent in cell 7 due to the ongoing Fe-oxide reduction. The net As release rates can be compared to the net As release rates derived from the profiles in Postma et al. (2007) which vary between ~ 0.4 and $-0.2 \mu\text{M/y}$ and are consistent with the values derived here. The model indicated that the dissolved arsenic is mostly As(III) (average concentration = $6.5 \times 10^{-7} \text{ M}$), whereas As(V) has very low concentrations (average of $8.0 \times 10^{-14} \text{ M}$). This result is in agreement with the reductive dissolution mechanism (Ravenscroft et al. 2009).

4. Discussion

4.1. Processes Governing Dissolved Carbonate, Iron and Manganese Concentrations

The supersaturation observed for carbonates can be related to the aquifer mineralogical composition, since sediments have an alpine origin and mainly derive from limestone formations (Ori 1993), combined with an internal production of inorganic carbon from OM oxidation. The equilibrium diagrams for calcite and dolomite (Figure 3a & b) show a different slope between the equilibrium line and the alignment of the measured data. This indicates that the dissolved carbonate species are not controlled by the calcite and dolomite dissolution equilibrium. A likely cause of this supersaturation and lack of alignment could be the presence of kinetic inhibitors (Appelo and Postma 2005) in the form of organic acids (Davis et al. 2000) and phosphates (Walter and Hanor 1979).

On the other hand, the data on the rhodochrosite plot (Figure 3c) are well aligned along the equilibrium line, with the exception of those from Uox and Umix that are subsaturated and some Ured and S points that are supersaturated (with an SI up to 0.3-0.5). If we assume an origin of the rhodochrosite from the reduction of Mn-oxides and the production of dissolved carbonate from the oxidation of OM, the subsaturation in Uox and Umix could be explained by unfavorable condition for Mn-oxide reduction. The presence of higher manganese concentration due to Mn-oxides reduction and a likely kinetic inhibition of the ongoing rhodochrosite precipitation could explain the supersaturation in Ured and aquifer S. The alignment with the equilibrium line for the underlying aquifers suggests that rhodochrosite equilibrium controls the dissolved carbonate and manganese concentrations in the deeper part of the system.

The siderite plot (Figure 3d) looks similar to that of rhodochrosite although the alignment with the equilibrium line is less clear. Points from Uox and Umix are subsaturated whereas those from Ured and aquifer S are supersaturated with an SI \sim 0.8. Similarly to rhodochrosite, the supersaturation could be due to higher concentration of Fe^{2+} generated by the Fe-oxides reduction and a likely kinetic inhibition of the siderite precipitation. As depth increases, FeS precipitation could take place and lower the Fe^{2+} concentration. The point from Ured that is subsaturated (well 4) is the only one classified as anoxic with manganese reduction (Rotiroti et al. 2014).

The system of processes likely governing the Fe concentration are combined in the plot in Figure 4a. The alignment of measured data along an equilibrium line could mean that the concentration of Fe^{2+} , in relation to the pH, is most likely governed by concomitant Fe-oxide and sulfate reduction and FeS precipitation. In particular, the alignment to the equilibrium line corresponding to microcrystalline goethite is in accordance with the finding of limonite in the geological log reported by Martinelli et al. (2005), that is representative of the depositional system of the study area. Limonite is a mixture of Fe-oxides in varying composition where goethite is generally abundant (Degens 1965). The points that are not clearly aligned to the microcrystalline goethite line are mainly from Uox and Umix (and well 4 from Ured), where presumably sulfate reduction is not

occurring due to the presence of more oxidized conditions. Moreover, the plot of the line for siderite equilibrium alone (see the Supporting Information) shows no clear alignment to the field data.

Therefore, this equilibrium probably has a minor effect on the relation between Fe^{2+} and pH.

Results of the reactive transport model agree with these assumptions since the rates of Fe-oxide and sulfate precipitation and FeS precipitation have a similar profile with a peak in the same cell (i.e., cell 4). Moreover, the optimal value of logK of the Fe-oxide resulted in the model (i.e., $\log K = -0.11$) is in the stability range of goethite and approaches that for the microcrystalline goethite (i.e., $\log K = 0.78$) for which a lot of field data seem to be at equilibrium.

Concerning the Mn, the plot in Figure 3b suggests that the Mn-oxide reduction is likely far from equilibrium playing a minor role in controlling the Mn^{2+} concentration in groundwater. On the other hand, the plot of the equilibrium line for rhodochrosite precipitation (blue line) shows a clear alignment with the measured data. This confirms the assumption that rhodochrosite precipitation plays a key role in the control of dissolved manganese concentrations in the study area. Reduction of Mn-oxides does not appear to occur near equilibrium, perhaps because the high thermodynamic energy yield would imply unrealistically low concentrations of e.g. H_2 similar to what has been shown for dechlorination (Heimann and Jakobsen 2006). Alternatively, at the low pe of the system, equilibrium with the Mn-oxides would require enormously high Mn^{2+} values, that can never be obtained because the Mn^{2+} concentration is limited by the solubility of rhodochrosite. These assumptions are also supported by the model results since a good match between modeled and measured data was obtained considering only the rhodochrosite precipitation as controlled by equilibrium and the Mn-oxide reduction as an irreversible reaction.

In summary, the Fe^{2+} concentration in the aquifer system in Cremona seems to be governed by the simultaneous equilibrium between Fe-oxide and sulfate reduction and FeS and (maybe) siderite precipitation. The presence of Fe-oxides with medium stability in the system may allow the sulfate reduction to be energetically feasible, so the two reduction processes can take place simultaneously

(Postma and Jakobsen 1996). The Mn^{2+} and dissolved carbonate concentrations seem to be controlled by rhodochrosite precipitation close to equilibrium.

4.2. Peaty aquitard as driver of As release

The optimal C/N ratio of OM used in the model (i.e., 23.6) is close to the value of 22.3 reported for peat by Clark and Fritz (1997) and to the soil C/N ratio of 25.73 reported by Aitkenhead and McDowell (2000) for the boreal/peat mix biome. This, in addition to the finding of peat in several lithologs (Figure 2), confirms that the likely origin of reactive OM in the system is peat deposits. More precisely, the analysis of lithologs indicated that peats are associated with low-permeability (clays and silts) and semipermeable (silty sands) layers acting as aquitards. Therefore, peaty aquitards seem to be a source of reactive OM in the system.

The model fitted to the measured data showed that the whole hydrochemistry was influenced by the flow of groundwater through the shallowest aquitard U/S (20-30 m b.s.). Indeed below 30 m b.s. the OC degradation, the Fe-oxide and sulfate reduction and the net As release rates all peak. This indicates that the aquitard U/S provided the reactive OM capable of driving the As release. The fact that the aforementioned peaks were registered just downstream the aquitard and not within it may indicate that part of the OM contained in the aquitard could be transported as DOC into the underlying aquifer.

The fitted model also showed that the two shallower aquitards (i.e., U/S and S/C1) have a different capacity in driving the As release: the net rate of As release is $0.28 \mu M/y$ in aquitard U/S (cell 3) and $0.07 \mu M/y$ in aquitard S/C1 (average of cells 7-8). This could be related to a different reactivity of the OM contained in the two aquitards, indeed aquitard U/S is more shallow and young, and thus, most likely has more reactive (Postma et al. 2012) OM. The OM reactivity of the aquitard U/S simulated in the model is in line with literature data: its OC degradation rate is $0.4 mM/y$ (cell 3)

that is in the range of Pleistocene age reported by Jakobsen and Postma (1994). This is consistent with the sediments below 20 m b.s. being most likely of Pleistocene age (Rotiroti et al. 2014).

4.3. Precipitation of FeS as trap for As

The alignment of most measured data along the equilibrium line in Figure 3a, that involved the FeS precipitation together with Fe-oxide and sulfate reduction, showed that suitable conditions for the precipitation of authigenic iron sulfides exist in the aquifer system in Cremona. This is confirmed also by the model results that showed a correspondence between the peak of FeS precipitation and those of the Fe-oxide and sulfate reduction rates.

The co-precipitation of As in FeS simulated by the model gave good results in term of fitting measured As concentrations imposing an initial increasing As(III)/Fe molar ratio which then reaches a constant value.

This could reflect that pure FeS likely only precipitates at the early stage of FeS precipitation whereas, with increasing As concentration, As may start to co-precipitate with a likely kinetic control, then, when a steady state is reached, it may co-precipitate with a constant As(III)/Fe ratio. The role of the co-precipitation of As in FeS in the dynamics of dissolved As is described in more detail in Figure 6 that compares model results for precipitation of pure FeS and the precipitation of FeS with As as an impurity. Without As in the FeS the modeled As concentration increases over depth giving a very poor fit (Jessen et al. 2008).

4.4. Implication for As Mobility

The occurrence of Fe-oxide and sulfate reduction and FeS precipitation close to a simultaneous equilibrium seems to have important implications on As mobility in the aquifer system studied. Indeed, the concomitant equilibrium of the processes that represents the likely source (Fe-oxide

reduction) and sink (FeS precipitation) of As may give some constraints to its mobility. Model results showed that, due to this simultaneous equilibrium, the highest net As precipitation rate (0.32 $\mu\text{M}/\text{y}$ in cell 5) is just downstream the highest net As release rate (0.32 $\mu\text{M}/\text{y}$ in cell 6). This may indicate that, under the aforementioned concomitant equilibrium, As could be released and subsequently trapped over a short distance, limiting the extent of its contamination close to the source of OM, that is the driver of its release. In other words, we speculate that the extent of As contamination in groundwater could be attenuated close to the OM source that drives its release - if Fe-oxide and sulfate reduction and FeS precipitation approach a simultaneous equilibrium. Considering the peaty aquitard as source of OM, the As contamination should be more severe in the portion of aquifer just downstream the aquitard. This seems to be confirmed by the measured and modeled As concentrations in aquifer S that shows a decrease from its top (adjacent to aquitard U/S) to its bottom.

5. Conclusions

This work presented a reactive transport modeling aiming at quantifying and testing the feasibility of a conceptual model for As release and attenuation in the Po Plain. Model results seem to support the following hypothesis:

- a) the OM contained and/or derived from peaty aquitards is the likely driver of the As release from Fe-oxides, leading to contamination in downstream aquifers;
- b) the FeS formed by the products of Fe-oxide and sulfate reduction, that likely occur close to a simultaneous equilibrium, traps the dissolved As lowering its concentration.

Other aspects emerging from this study, that may have implications in other alluvial basins worldwide with analogous hydrogeological and hydrogeochemical features:

- a) shallow rather than deep peaty aquitards seem to have greater importance in driving the As release since they likely contain young, and thus, more reactive OM;

- b) the occurrence of Fe-oxide and sulfate reduction and FeS precipitation close to a concomitant equilibrium may restrict the As mobility in groundwater, attenuating As contamination just downstream the source of OM that drives its release.

Acknowledgments

Funding was provided by Province of Cremona within the scientific collaboration 7-19-2009100-2 and by Italian Ministry of Education, University and Research within the PRIN-2008 project 2008YP85ZH.

We thank Andrea Azzoni, Barbara Pisaroni and Giuseppina Demicheli of Province of Cremona for supporting this study. The Gocad Research Group and Paradigm Geophysical are acknowledged for welcoming the University of Milano-Bicocca into the Gocad Consortium (<http://www.Gocad.org>). We also wish to thank an anonymous reviewer for useful comments and suggestions.

Appendix A. Supporting Information

Details on the reconstruction of the 3D distribution of textural facies, hydraulic conductivity and effective porosity, the stoichiometry of redox and mineral dissolution reactions considered, the reactive transport model settings, additional figures and tables are the supporting information related to this article.

References

- Aitkenhead JA, McDowell WH (2000) Soil C:N ratio as a predictor of annual riverine DOC flux at local and global scales. *Global Biogeochem. Cy.* 14 (1):127-138.
doi:10.1029/1999gb900083

- Amorosi A, Centineo MC, Colalongo ML, Fiorini F (2005) Millennial-scale depositional cycles from the Holocene of the Po Plain, Italy. *Mar. Geol.* 222–223:7-18.
doi:10.1016/j.margeo.2005.06.041
- Amorosi A, Pavesi M, Ricci Lucchi M, Sarti G, Piccin A (2008) Climatic signature of cyclic fluvial architecture from the Quaternary of the central Po Plain, Italy. *Sediment. Geol.* 209 (1–4):58-68. doi:10.1016/j.sedgeo.2008.06.010
- Appelo CAJ, Postma D (2005) *Geochemistry, groundwater and pollution 2edn.* Balkema Publishers, Leiden.
- Ball JW, Nordstrom DK (1991) *WATEQ4F - User's manual with revised thermodynamic data base and test cases for calculating speciation of major, trace and redox elements in natural waters.* USGS Open-File Report 90-129, Reston.
- Baraldi F, Castaldini D, Marchetti M (2001) Geomorphological impact assessment in the River Mincio plain (Province of Mantova, Northern Italy). In: Marchetti M, Rivas V (Eds.) *Geomorphology and Environmental Impact Assessment.* Balkema, Rotterdam, pp. 7-30.
- Bonomi T (2009) Database development and 3D modeling of textural variations in heterogeneous, unconsolidated aquifer media: Application to the Milan plain. *Comput. Geosci.* 35 (1):134-145. doi:10.1016/j.cageo.2007.09.006
- Bonomi T, Fumagalli M, Rotiroli M, Bellani A, Cavallin A (2014) Banca dati idrogeologica TANGRAM©: strumento per elaborazioni quantitative di dati per la valutazione delle acque sotterranee (The hydrogeological well database TANGRAM©: a tool for data processing to support groundwater assessment). *Acq. Sott.-Ital. J. Groundwater* 3 (2/136):35-45.
doi:10.7343/AS-072-14-0098
- Buschmann J, Berg M (2009) Impact of sulfate reduction on the scale of arsenic contamination in groundwater of the Mekong, Bengal and Red River deltas. *Appl. Geochem.* 24 (7):1278-1286. doi:10.1016/j.apgeochem.2009.04.002

- Carraro A, Fabbri P, Giaretta A, Peruzzo L, Tateo F, Tellini F (2013) Arsenic anomalies in shallow Venetian Plain (Northeast Italy) groundwater. *Environ. Earth. Sci.* 70 (7):3067-3084. doi:10.1007/s12665-013-2367-2
- Castelli A, Chiesa S, Deriu G, Pezzerà G, Vescovi E, Zanotti M, Zonca B (2005) Note sulla presenza di arsenico nel sottosuolo e nelle acque sotterranee della Lombardia (Occurrence of arsenic in aquifer sediments and groundwater in Lombardy region). In: Scialoja MG (Eds.) *Presenza e diffusione dell'arsenico nel sottosuolo e nelle risorse idriche italiane (Occurrence and distribution of arsenic in sediments and water resources of Italy)*. Arpa Emilia-Romagna, Bologna, pp. 39-50.
- Clark I, Fritz P (1997) *Environmental Isotopes in Hydrogeology*. Lewis Publishers, New York.
- Cornell RM, Schwertmann U (2003) *The iron oxides*. 2 edn. Wiley-VCH, Weinheim.
- Cubadda F, Ciardullo S, D'Amato M, Raggi A, Aureli F, Carcea M (2010) Arsenic Contamination of the Environment–Food Chain: A Survey on Wheat as a Test Plant To Investigate Phytoavailable Arsenic in Italian Agricultural Soils and as a Source of Inorganic Arsenic in the Diet. *J. Agric. Food Chem.* 58 (18):10176-10183. doi:10.1021/jf102084p
- Davis KJ, Dove PM, De Yoreo JJ (2000) The Role of Mg²⁺ as an Impurity in Calcite Growth. *Science* 290 (5494):1134-1137. doi:10.1126/science.290.5494.1134
- de la Fuente C, Clemente R, Albuquerque JA, Vélez D, Bernal MP (2010) Implications of the Use of As-Rich Groundwater for Agricultural Purposes and the Effects of Soil Amendments on As Solubility. *Environ. Sci. Technol.* 44 (24):9463-9469. doi:10.1021/es102012s
- Degens ET (1965) *Geochemistry of sediments: a brief survey*. Prentice-Hall, Englewood Cliffs.
- Desbarats AJ, Koenig CEM, Pal T, Mukherjee PK, Beckie RD (2014) Groundwater flow dynamics and arsenic source characterization in an aquifer system of West Bengal, India. *Water Resour. Res.* 50 (6):4974-5002. doi:10.1002/2013wr014034
- Díaz OP, Leyton I, Muñoz O, Núñez N, Devesa V, Súañer MA, Vélez D, Montoro R (2004) Contribution of Water, Bread, and Vegetables (Raw and Cooked) to Dietary Intake of

- Inorganic Arsenic in a Rural Village of Northern Chile. *J. Agric. Food Chem.* 52 (6):1773-1779. doi:10.1021/jf035168t
- Fabbri P, Trevisani S (2005) A Geostatistical Simulation Approach to a Pollution Case in Northeastern Italy. *Math. Geol.* 37 (6):569-586. doi:10.1007/s11004-005-7307-6
- Fendorf S, Michael HA, van Geen A (2010) Spatial and Temporal Variations of Groundwater Arsenic in South and Southeast Asia. *Science* 328 (5982):1123-1127. doi:10.1126/science.1172974
- Gelhar LW, Welty C, Rehfeldt KR (1992) A critical review of data on field-scale dispersion in aquifers. *Water Resour. Res.* 28 (7):1955-1974. doi:10.1029/92wr00607
- Guffanti S, Pilla G, Sacchi E, Ughini S (2010) Characterization of the quality and origin of groundwater of Lodigiano (Northern Italy) with hydrochemical and isotopic instruments. *Ital. J. Eng. Geol. Envir.* 1:65-78.
- Heimann AC, Jakobsen R (2006) Experimental Evidence for a Lack of Thermodynamic Control on Hydrogen Concentrations during Anaerobic Degradation of Chlorinated Ethenes. *Environ. Sci. Technol.* 40 (11):3501-3507. doi:10.1021/es052320u
- Huq SMI, Joardar JC, Parvin S, Correll R, Naidu R (2006) Arsenic contamination in food-chain: Transfer of arsenic into food materials through groundwater irrigation. *J. Health Popul. Nutr.* 24 (3):305-316.
- Jakobsen R, Cold L (2007) Geochemistry at the sulfate reduction–methanogenesis transition zone in an anoxic aquifer—A partial equilibrium interpretation using 2D reactive transport modeling. *Geochim. Cosmochim. Acta* 71 (8):1949-1966. doi:10.1016/j.gca.2007.01.013
- Jakobsen R, Postma D (1994) In situ rates of sulfate reduction in an aquifer (Rømø, Denmark) and implications for the reactivity of organic matter. *Geology* 22 (12):1101-1106. doi:10.1130/0091-7613(1994)022<1103:isrosr>2.3.co;2

- Jakobsen R, Postma D (1999) Redox zoning, rates of sulfate reduction and interactions with Fe-reduction and methanogenesis in a shallow sandy aquifer, Rømø, Denmark. *Geochim. Cosmochim. Acta* 63 (1):137-151. doi:10.1016/S0016-7037(98)00272-5
- Jessen S, Larsen F, Postma D, Viet PH, Ha NT, Nhan PQ, Nhan DD, Duc MT, Hue NTM, Huy TD, Luu TT, Ha DH, Jakobsen R (2008) Palaeo-hydrogeological control on groundwater As levels in Red River delta, Vietnam. *Appl. Geochem.* 23 (11):3116-3126. doi:10.1016/j.apgeochem.2008.06.015
- Jessen S, Postma D, Larsen F, Nhan PQ, Hoa LQ, Trang PTK, Long TV, Viet PH, Jakobsen R (2012) Surface complexation modeling of groundwater arsenic mobility: Results of a forced gradient experiment in a Red River flood plain aquifer, Vietnam. *Geochim. Cosmochim. Acta* 98 (0):186-201. doi:10.1016/j.gca.2012.07.014
- Lowers HA, Breit GN, Foster AL, Whitney J, Yount J, Uddin MN, Muneem AA (2007) Arsenic incorporation into authigenic pyrite, Bengal Basin sediment, Bangladesh. *Geochim. Cosmochim. Acta* 71 (11):2699-2717. doi:10.1016/j.gca.2007.03.022
- Marchina C, Bianchini G, Natali C, Pennisi M, Colombani N, Tassinari R, Knoeller K (2015) The Po river water from the Alps to the Adriatic Sea (Italy): new insights from geochemical and isotopic ($\delta^{18}\text{O}$ - δD) data. *Environ. Sci. Pollut. Res.* 22 (7):5184-5203. doi:10.1007/s11356-014-3750-6
- Martinelli M, Marcaccio M, Farina M, Canepa P, Cantagalli L, Billi L (2005) L'arsenico nei sedimenti profondi della pianura emiliano-romagnola: prime evidenze (Arsenic in the deep sediments of Emilia-Romagna plain: first evidence). In: Scialoja MG (Eds.) *Presenza e diffusione dell'arsenico nel sottosuolo e nelle risorse idriche italiane (Occurrence and distribution of arsenic in sediments and water resources of Italy)*. ARPA Emilia-Romagna, Bologna, pp 215-224.
- McArthur JM, Banerjee DM, Hudson-Edwards KA, Mishra R, Purohit R, Ravenscroft P, Cronin A, Howarth RJ, Chatterjee A, Talukder T, Lowry D, Houghton S, Chadha DK (2004) Natural

organic matter in sedimentary basins and its relation to arsenic in anoxic ground water: the example of West Bengal and its worldwide implications. *Appl. Geochem.* 19 (8):1255-1293. doi:10.1016/j.apgeochem.2004.02.001

Miola A, Bondesan A, Corain L, Favaretto S, Mozzi P, Piovan S, Sostizzo I (2006) Wetlands in the Venetian Po Plain (northeastern Italy) during the Last Glacial Maximum: Interplay between vegetation, hydrology and sedimentary environment. *Rev. Palaeobot. Palynol.* 141 (1–2):53-81. doi:10.1016/j.revpalbo.2006.03.016

Molinari A, Guadagnini L, Marcaccio M, Straface S, Sanchez-Vila X, Guadagnini A (2013) Arsenic release from deep natural solid matrices under experimentally controlled redox conditions. *Sci. Total Environ.* 444:231-240. doi:10.1016/j.scitotenv.2012.11.093

Ori GG (1993) Continental depositional systems of the Quaternary of the Po Plain (northern Italy). *Sediment. Geol.* 83 (1–2):1-14. doi:10.1016/S0037-0738(10)80001-6

Paradigm (Eds.) (2009) GOCAD 2009 User Guide. Part IX Reservoir Modeling. Paradigm Ltd., Houston.

Parkhurst DL, Appelo CAJ (2013) Description of input and examples for PHREEQC version 3-A computer program for speciation, batch-reaction, one-dimensional transport, and inverse geochemical calculations. In: *USGS Techniques and Methods, Book 6, Modeling Techniques*. USGS, Reston, Chapter 43.

Planer-Friedrich B, Härtig C, Lissner H, Steinborn J, Süß E, Qumrul Hassan M, Zahid A, Alam M, Merkel B (2012) Organic carbon mobilization in a Bangladesh aquifer explained by seasonal monsoon-driven storativity changes. *Appl. Geochem.* 27 (12):2324-2334. doi:10.1016/j.apgeochem.2012.08.005

Postma D, Jakobsen R (1996) Redox zonation: Equilibrium constraints on the Fe(III)/SO₄-reduction interface. *Geochim. Cosmochim. Acta* 60 (17):3169-3175. doi:10.1016/0016-7037(96)00156-1

- Postma D, Larsen F, Minh Hue NT, Duc MT, Viet PH, Nhan PQ, Jessen S (2007) Arsenic in groundwater of the Red River floodplain, Vietnam: Controlling geochemical processes and reactive transport modeling. *Geochim. Cosmochim. Acta* 71 (21):5054-5071.
doi:10.1016/j.gca.2007.08.020
- Postma D, Larsen F, Thai NT, Trang PTK, Jakobsen R, Nhan PQ, Long TV, Viet PH, Murray AS (2012) Groundwater arsenic concentrations in Vietnam controlled by sediment age. *Nature Geosci.* 5 (9):656-661. doi: 10.1038/ngeo1540
- Ravenscroft P, Brammer H, Richards K (2009) *Arsenic Pollution: A Global Synthesis*. Wiley-Blackwell, Chichester.
- Redfield AC (1934) On the proportions of organic derivations in sea water and their relation to the composition of plankton. In: Daniel RJ (Eds.) *James Johnstone Memorial Volume*. University Press of Liverpool, Liverpool, pp 177–192.
- Root RA, Vlassopoulos D, Rivera NA, Rafferty MT, Andrews C, O’Day PA (2009) Speciation and natural attenuation of arsenic and iron in a tidally influenced shallow aquifer. *Geochim. Cosmochim. Acta* 73 (19):5528-5553. doi:10.1016/j.gca.2009.06.025
- Rotiroti M, Fumagalli L (2013) Derivation of preliminary natural background levels for naturally Mn, Fe, As and NH_4^+ rich groundwater: the case study of Cremona area (Northern Italy). *Rend. Online Soc. Geol. It.* 24:284-286.
- Rotiroti M, Sacchi E, Fumagalli L, Bonomi T (2014) Origin of arsenic in groundwater from the multi-layer aquifer in Cremona (northern Italy). *Environ. Sci. Technol.* 48 (10):5395–5403.
doi:10.1021/es405805v
- Sciarra A, Cinti D, Pizzino L, Procesi M, Voltattorni N, Mecozzi S, Quattrocchi F (2013) Geochemistry of shallow aquifers and soil gas surveys in a feasibility study at the Rivara natural gas storage site (Po Plain, Northern Italy). *Appl. Geochem.* 34:3-22.
doi:10.1016/j.apgeochem.2012.11.008

- Sharma AK, Tjell JC, Sloth JJ, Holm PE (2014) Review of arsenic contamination, exposure through water and food and low cost mitigation options for rural areas. *Appl. Geochem.* 41:11-33.
doi:10.1016/j.apgeochem.2013.11.012
- Sigfusson B, Gislason SR, Meharg AA (2011) A field and reactive transport model study of arsenic in a basaltic rock aquifer. *Appl. Geochem.* 26 (4):553-564.
doi:10.1016/j.apgeochem.2011.01.013
- Sommella A, Deacon C, Norton G, Pigna M, Violante A, Meharg AA (2013) Total arsenic, inorganic arsenic, and other elements concentrations in Italian rice grain varies with origin and type. *Environ. Pollut.* 181:38-43. doi:10.1016/j.envpol.2013.05.045
- Torres-Escribano S, Leal M, Vélez D, Montoro R (2008) Total and Inorganic Arsenic Concentrations in Rice Sold in Spain, Effect of Cooking, and Risk Assessments. *Environ. Sci. Technol.* 42 (10):3867-3872. doi:10.1021/es071516m
- Toscani L, Boschetti T, Maffini M, Barbieri M, Mucchino C (2007) The groundwaters of Fontevivo (Parma Province, Italy): redox processes and mixing with brine waters. *Geochem.-Explor. Env. A.* 7 (1):23-40. doi:10.1144/1467-7873/06-112
- Walter LM, Hanor JS (1979) Effect of orthophosphate on the dissolution kinetics of biogenic magnesian calcites. *Geochim. Cosmochim. Acta* 43 (8):1377-1385. doi:10.1016/0016-7037(79)90128-5
- Zavatti A, Attramini D, Bonazzi A, Boraldi V, Malagò R, Martinelli G, Naldi S, Patrizi G, Pezzera G, Vandini W, Venturini L, Zuppi GM (1995) La presenza di Arsenico nelle acque sotterranee della Pianura Padana: evidenze ambientali e ipotesi geochimiche (Occurrence of groundwater arsenic in the Po Plain: environmental evidences and geochemical hypothesis). *Quad. Geol. Appl.* S2:2.301-2.326.

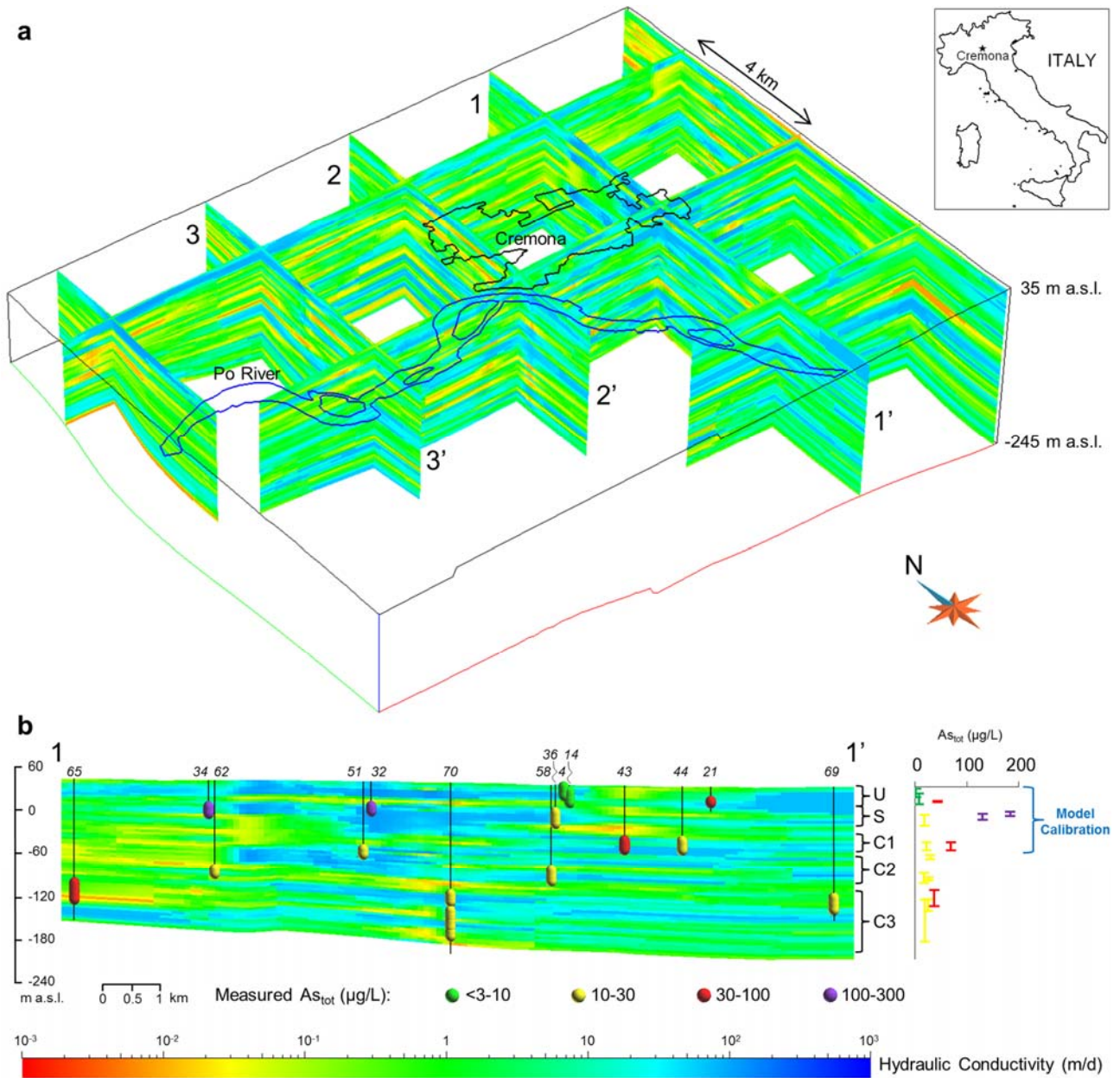


Figure 1. (a) 3D reconstruction of K (m/d) in the study area. (b) Measured As in wells from the eastern part of the study area projected onto the cross-section 1-1' (see the Supporting Information for well location); symbol length corresponds to well screen interval. Green symbols: $[As] < \text{WHO limit}$; yellow symbols: $[As] < 3 \times \text{WHO limit}$; red symbols: $[As] < 10 \times \text{WHO limit}$; purple symbols: $[As] < 30 \times \text{WHO limit}$.

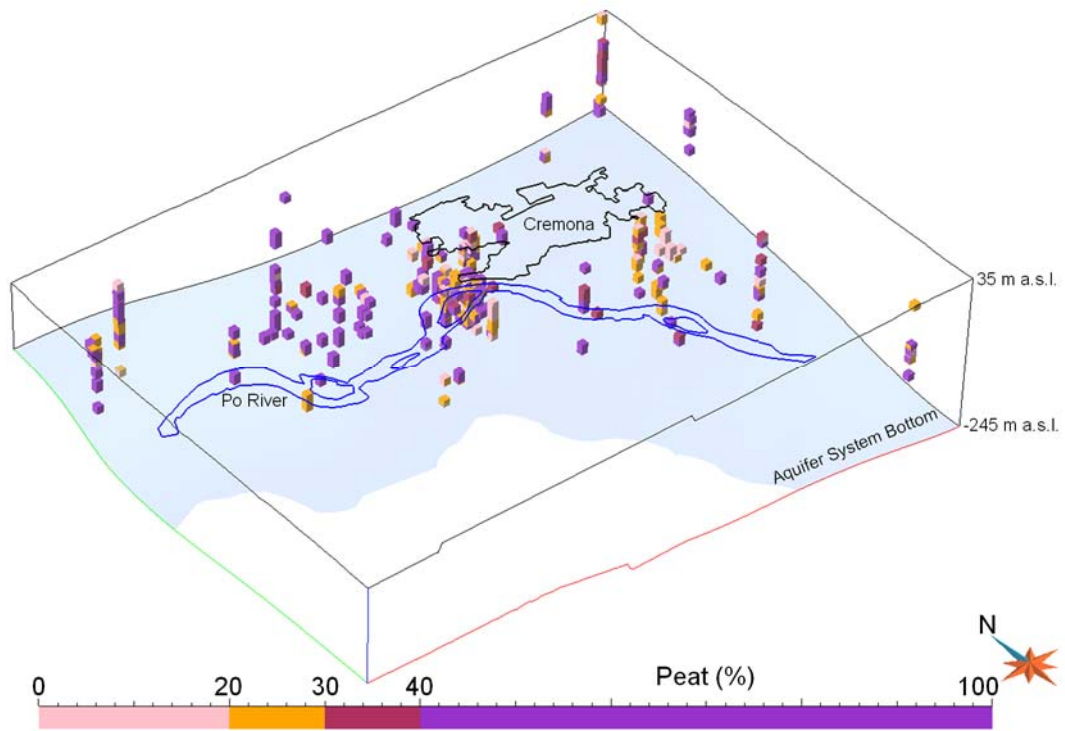


Figure 2. Presence and content of peat in the collected lithologies; classes of peat content (%) are based on the 25th (20%), 50th (30%) and 75th (40%) percentiles of the data; the white part of the box bottom is outside the model.

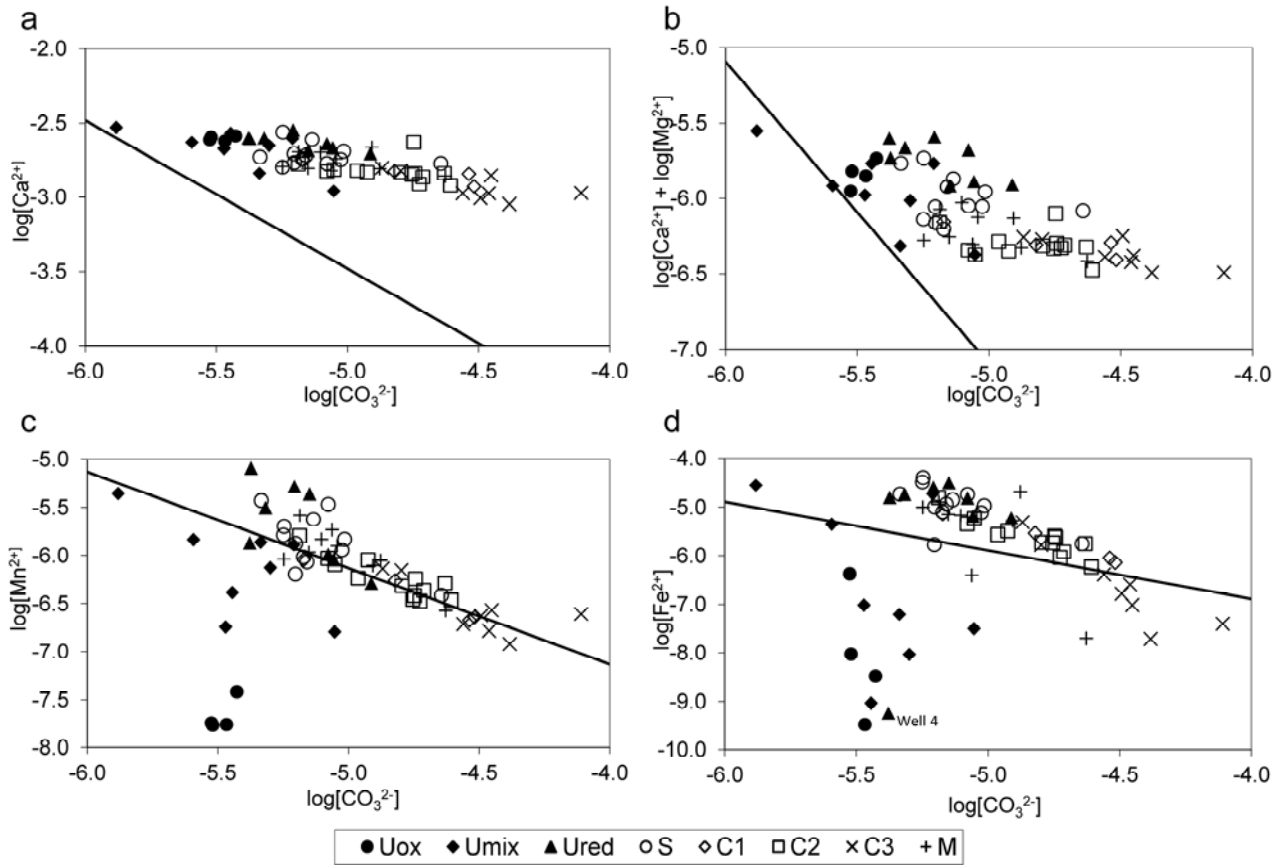


Figure 3. Chemical equilibrium diagram for dissolution/precipitation of (a) calcite, (b) dolomite, (c) rhodochrosite and (d) siderite; solid lines are equilibrium lines. Uox: oxidized zone of aquifer U; Umix: mixed class zone of aquifer U; Ured: reduced zone of aquifer U; S: aquifer S; C1: aquifer C1; C2: aquifer C2; C3: aquifer C3; M: multiaquifer.

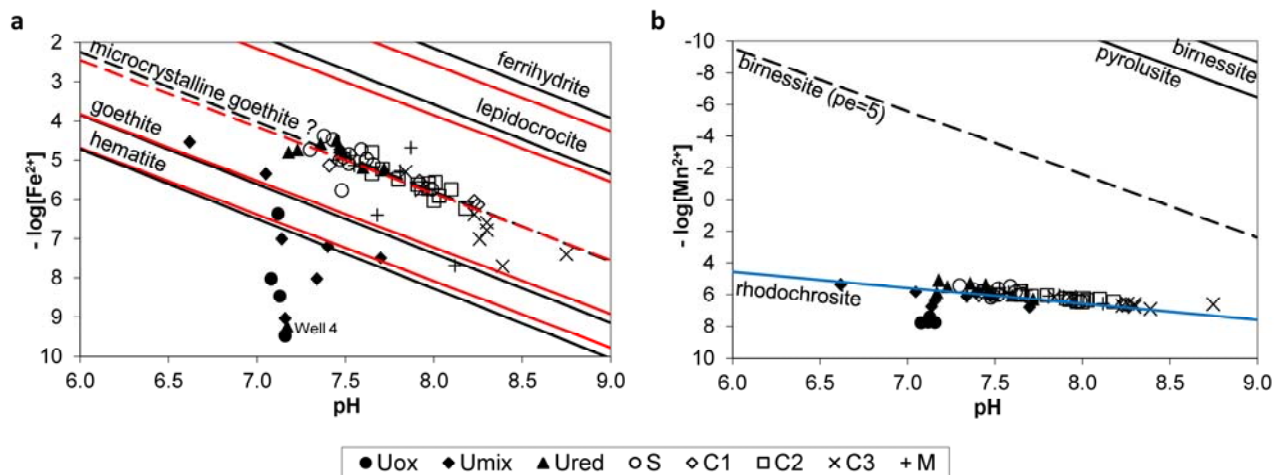


Figure 4. Equilibrium diagrams of (a) the simultaneous equilibrium of Fe-oxide and sulfate reduction and FeS precipitation (black lines) and siderite precipitation (red lines) and (b) the sole equilibrium of Mn-oxides reduction (black lines) and rhodochrosite precipitation (blue line). See the Supporting Information for equilibrium line equations and details. Uox: oxidized zone of aquifer U; Umix: mixed class zone of aquifer U; Ured: reduced zone of aquifer U; S: aquifer S; C1: aquifer C1; C2: aquifer C2; C3: aquifer C3; M: multiaquifer.

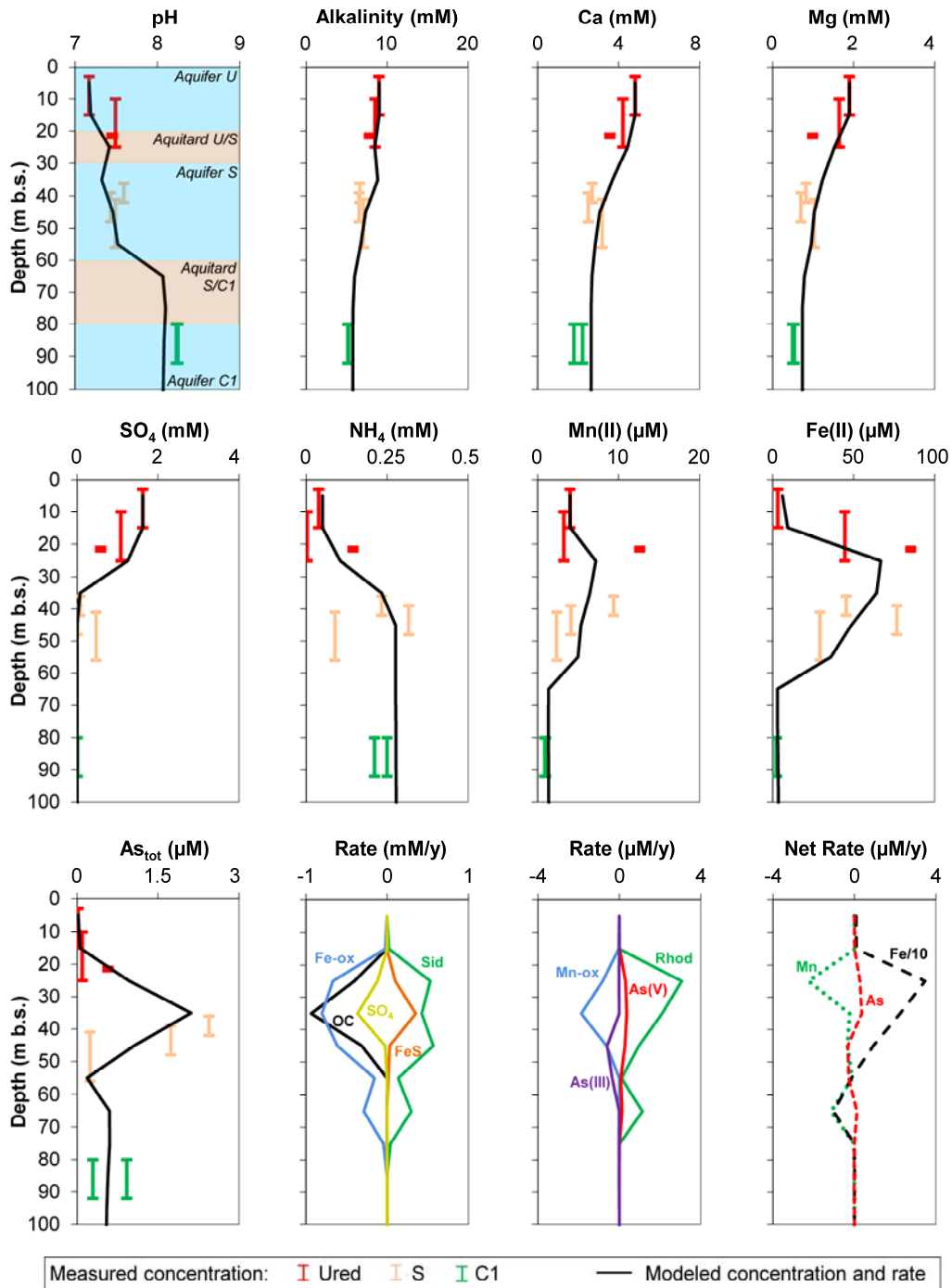


Figure 5. Measured and modeled molar concentrations of some major ions and redox sensitive species and modeled rates over depth; symbol length corresponds to well screen interval; negative rates indicate consumption, positive precipitation; negative As rates indicate As sequestration, positive As release; negative net rates indicate net precipitation, positive net release. Ured: reduced zone of aquifer U; S: aquifer S; C1: aquifer C1; Fe-ox: Fe-oxide reduction; OC: organic carbon consumption; SO₄: sulfate reduction; Sid: siderite precipitation; FeS: iron sulfide precipitation; Mn-ox: Mn-oxide reduction; Rhod: rhodochrosite precipitation; As(V): As(V) release; As(III): As(III) sequestration.

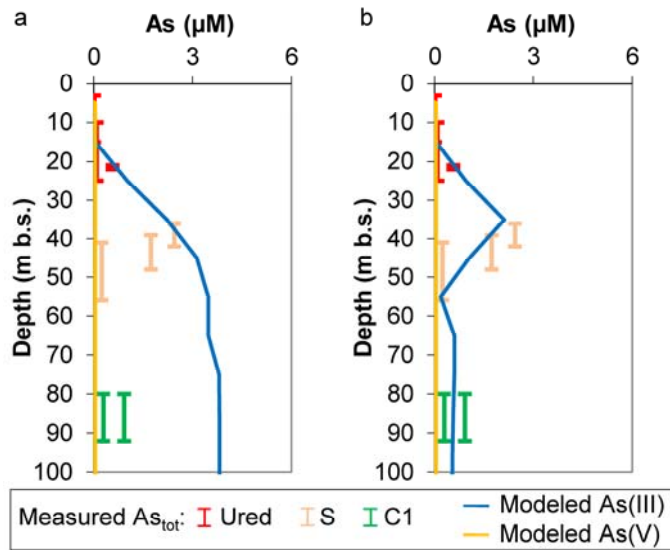


Figure 6. Comparison of model results of As(III) and As(V) concentrations imposing (a) the sole precipitation of pure FeS and (b) the precipitation of FeS with trace As; symbol length corresponds to well screen interval. Ured: reduced zone of aquifer U; S: aquifer S; C1: aquifer C1.

Table 1. Geometries and corresponding hydrogeological units of the 1D reactive transport model and resulting rates ($\mu\text{M}/\text{y}$) of OC consumption, As(V) release from Fe-oxide and As(III) co-precipitation in FeS and As(III)/Fe molar ratio in FeS.

Cell	Depth (m b.s.)	Unit	OC rate ^a	As(V) rate ^b	As(III) rate ^b	Net As rate ^{b,c}	As(III)/Fe in FeS
1	0-10	aquifer U	-3.12	4.2×10^{-4}	0	4.2×10^{-4}	no FeS prec.
2	10-20		-3.12	0.01	0	0.01	no FeS prec.
3	20-30	aquitard U/S	-404.99	0.30	-0.02	0.28	2.0×10^{-4}
4	30-40	aquifer S	-934.58	0.36	0	0.36	0
5	40-50		-311.53	0.28	-0.60	-0.32	1.9×10^{-2}
6	50-60		-3.12	0.07	-0.35	-0.28	2.0×10^{-2}
7	60-70	aquitard S/C1	-3.12	0.13	0	0.13	no FeS prec.
8	70-80		-3.12	0.02	-0.02	1.6×10^{-3}	2.0×10^{-2}
9	80-90	aquifer C1	-3.12	3.0×10^{-4}	-0.01	-0.01	2.0×10^{-2}
10	90-100		-3.12	1.7×10^{-4}	-0.01	-0.01	2.0×10^{-2}
11	100-110		-3.12	1.2×10^{-4}	-3.7×10^{-3}	-3.6×10^{-3}	2.0×10^{-2}
12	110-120	aquitard C1/C2	-3.12	1.5×10^{-4}	-1.9×10^{-3}	-1.8×10^{-3}	2.0×10^{-2}

^anegative values indicate consumption.

^bnegative values indicate precipitation, positive release.

^ccalculated considering the reductive dissolution of Fe-oxide with trace As(V) as source and the co-precipitation of As(III) in FeS as sink.